Int. J. Heat Mass Transfer. Vol. 32, No. 1, pp. 3–17, 1989
Printed in Great Britain

0017-9310/89 \$3.00+0.00
Pergamon Press plc

Heating, evaporation and combustion of a solid aerosol particle in a gas exposed to optical radiation

V. K. PUSTOVALOV and D. S. BOBUCHENKO
Byelorussian Polytechnical Institute, Minsk, 220027, U.S.S.R.

(*Received* 26 *March* 1987)

Abstract—Theoretical investigation is made of heating, evaporation and combustion of a small solid aerosol particle in a gas on exposure to intense optical radiation. The statement of the problem is given and the solution is obtained for quasi-steady-state diffusive–convective heat and mass transfer between the particle and the surrounding gas with allowance for the temperature dependence of the thermophysical and optical parameters and transfer coefficients. Based on numerical solution of the system of equations stated the evaporation of a metal particle in an inert gas and the combustion of a high-melting particle in air on exposure to optical radiation are considered. The time dependencies of the radius and temperature of the particle and of the process parameters are obtained. Comparison of some predicted results with experimental data is given.

1. INTRODUCTION

IN THE cases of non-linear intense optical radiation in aerosol media, optical probing of multi-phase media, etc., considerable interest is attached to the study of heating, evaporation and combustion of solid aerosol particles on their exposure to optical radiation. The fundamental difference between heating and evaporation of solid particles and of liquid droplets (for instance, water) by optical radiation [1] is the possibility of heating a solid particle up to the temperature $T_0 \gtrsim T_m$ which is higher than the initial temperature T_∞, $T_0 \gg T_\infty$ and $(T_0 - T_\infty)/T_\infty \gg 1$. Thus, $T_m = 933.6$ K for aluminium, $T_m = 2348$ K for boron, $T_m = 3653$ K for tungsten [2]; when $T_\infty = 300$ K, $(T_0 - T_\infty)/T_\infty \gtrsim 2$–$12$, whereas for water at $T_0 \sim 373$ K the ratio $(T_0 - T_\infty)/T_\infty \lesssim 0.3$. This leads to the necessity of taking into account the actual temperature dependence of optical and thermophysical parameters and of mass transfer coefficients for the particle material and surrounding gas in a wide temperature range; considering phase changes, investigating non-linear and non-isothermal heat and mass transfer of a particle with the surrounding gas. A number of problems of heating and evaporation of solid particles by optical radiation were previously considered theoretically [3–5]. However, in these works the temperature dependence of the coefficients of diffusion, D, and thermal conductivity, κ, in gas were taken in the form: $D \sim T^{3/2}$, $\kappa \sim T^{1/2}$ which differ markedly from the actual functions $D(T)$, $\kappa(T)$ [6] and which, with heating up to $T_0 \sim 3 \times 10^3$ K, underestimate the values of κ and D, i.e. underestimate heat and mass fluxes from a particle by a factor of about 5–6. References [3–5] disregarded an important temperature dependence of the thermophysical (heat capacity, density, etc.) and optical (refraction and absorption indices) parameters of the material. Moreover, diffusional evaporation of a solid particle was considered in refs. [3–5] using the isothermal approximation $(T_0 - T_\infty)/T_\infty < 1$, which does not hold for heating when $T_0 \gtrsim T_m$, and it is necessary to consider non-isothermal diffusion of vapour in the surrounding gas. No consideration was made of the energy characteristics of solid particles evaporating on exposure to radiation. Also worth noting are refs. [7, 8] which dealt with surface combustion of carbon particles in air under the action of optical radiation with diffusional removal of gaseous reaction products from the particle. It follows from the above that of great importance is the theoretical investigation of heating, phase changes, evaporation and combustion of solid (specifically, metallic) aerosol particles in gas exposed to intense optical radiation, taking a more correct account of the actual temperature dependence of thermophysical and optical parameters, etc. It is this investigation which is presented in this paper. A quasi-stationary solution is obtained for diffusive–convective heat and mass transfer of a particle with temperature dependence of diffusion and heat conduction coefficients. Comparison with experimental data is given. Consideration is made of heating, phase changes and evaporation of a spherical aluminium particle in an inert gas under the action of optical radiation. Heating, oxidation and combustion of a high-melting aerosol particle of boron by optical radiation are investigated.

2. STATEMENT OF THE PROBLEM

Suppose optical radiation with wavelength λ and energy flux density (intensity) $I_0(t)$ be incident, start-

NOMENCLATURE

C	heat capacity
c_i	concentration of ith component of gas mixture
C_p	heat capacity at constant pressure
D	coefficient of interdiffusion of gas mixture components
D_k	coefficient of oxidant diffusion through oxide film
E_0	chemical reaction activation energy
E_T	thermal energy of particle
h	oxide film thickness on a particle
I_0	optical radiation intensity
j	net mass flux density
j_ε	energy flux density
j_i	mass flux density of ith component
k	Boltzmann's constant, $1.38054 \times 10^{-23}\,\mathrm{J\,K^{-1}}$
K_{ab}	radiation absorption efficiency factor
K_{sc}	scattering efficiency factor
k_0	pre-exponent of chemical reaction rate
L	heat of unit mass evaporation
L_m	heat of unit mass melting
M	energy parameters characterizing contribution of separate processes into total energy balance of particle
m	mass of vapour molecule
n_λ	refractive index of particle material at the wavelength
p	pressure
Q	integral energy parameters characterizing radiation–particle interaction
q_p	energy generation due to chemical reaction
r_0	instantaneous radius of a particle
r	radiation coordinate
R_g	gas constant $[\mathrm{J\,K^{-1}\,kg^{-1}}]$
S	surface area of particle
T	temperature
T_0	temperature of a particle
T_m	melting temperature of particle material
T_b	boiling temperature of particle material
t	time
V	particle volume
v	velocity.

Greek symbols

α	condensation (evaporation) coefficient
ε	particle surface emissivity
κ_λ	absorption index of a particle at wavelength λ
κ	thermal conductivity
λ	optical radiation wavelength
ρ	density
ρ_{sat}	saturated vapor density of particle material at T_0
σ	Stefan–Boltzmann constant, $5.67 \times 10^{-8}\,\mathrm{J\,K^{-4}\,m^{-2}\,s^{-1}}$
ψ	thermal diffusivity.

Subscripts

ab	absorption
c	convection
ch	chemical
cond	conduction
d	diffusion
ev	evaporation
i	0, particle material in condensed state; 1, vapour particle material; 2, neutral gas; 3, gaseous oxidant; 4, gaseous products of chemical reaction
l	melted state of a particle
m	melting
max	maximum
n	normalized
ox	oxide in condensed state
rad	radiation
s	solid state of a particle
sat	saturation
sc	scattering
∞	initial value
$-$	value refers directly to the vicinity of the particle surface.

ing from time $t = 0$, on a solid spherical particle with the initial radius r_∞ and temperature T_∞ (equal to the surrounding gas temperature). The particle absorbs the radiation energy and becomes heated. Within the range $T_\infty < T_0 < T_m$, there is virtually no evaporation on the solid particle and it gives up its heat to the surrounding gas by conduction. Heat transfer between spherical and spheroidal particles, which absorb radiant energy, and the surrounding gas with no mass transfer was considered in refs. [9–11]. The processes of heating and heat transfer of a spherical particle are described by

$$\rho_0 C_0 \frac{\partial T}{\partial t} = \mathrm{div}\,(\kappa_0(T)\,\mathrm{grad}\,T) + q_0 \tag{1}$$

subject to the initial and boundary conditions

$$T(t=0) = T_\infty, \quad -\kappa_0(T)\,\mathrm{grad}\,T|_{r_0} = \bar{j}_\varepsilon, \quad T(r_0) = T_0 \tag{2}$$

where $\bar{j}_\varepsilon$ is the density of the net energy flux removed from the particle surface. The energy generation power density in the particle q_0 due to radiation energy absorption can be generally non-uniform throughout the particle volume, with the non-uniformity being dependent on λ, size and optical constants of the particle material. In many cases q_0 is virtually uniform throughout the particle volume (variations of q_0 relative to its mean value do not exceed 20–30%) [12]. In what follows, it will be assumed for simplicity that q_0 is constant throughout the particle volume. The characteristic time t_0 required for the development of a quasi-stationary temperature profile inside the particle is estimated from the formula: $t_0 \sim r_0^2/\psi_0$. For characteristic particle sizes $r_0 \sim 1$–$10\ \mu$m and $\psi_0 \sim 10^{-5}$–$10^{-4}\ \mathrm{m^2\ s^{-1}}$, $t_0 \sim 10^{-8}$–10^{-6} s, which are much smaller than the characteristic times of heating, evaporation and combustion of a particle, and the quasi-stationary equation (1) can be considered at $\partial T/\partial t = 0$. Analytical quasi-stationary solutions (1) and (2) with regard for power law and exponential temperature functions $\kappa_0(T)$ were obtained in ref. [9]. Thus, when $\kappa_0 = \kappa_{0\infty}(T/T_\infty)^{a_0}$, the quasi-stationary distribution inside of the particle at $q_0 = \text{const.}$ in a spherical coordinate system with the origin at the particle centre will be

$$a_0 \neq -1, T = T_0\left[1+\frac{q_0(a_0+1)T_\infty^{a_0}}{6\kappa_{0\infty}T_0^{a_0+1}}(r_0^2-r^2)\right]^{1/(a_0+1)}$$

$$a_0 = -1, \quad T = T_0\exp\left[\frac{q_0}{6\kappa_{0\infty}T_\infty}(r_0^2-r^2)\right]. \quad (3)$$

The terms $(q_0(a_0+1)T_\infty^{a_0}r_0^2)/(6\kappa_{0\infty}T_0^{a_0+1})$ and $q_0r_0^2/(6\kappa_{0\infty}T_\infty)$ in equations (3) characterize the non-uniformity of the temperature distribution inside of the particle and the difference between the temperature T at the centre $T(r = 0)$ and T_0 at the particle surface. Their estimates for characteristic values of the parameters showed that these expressions are much smaller than 1, and the approximation to the temperature which is uniform over the particle volume and which coincides with temperature T_0 of its surface, can be used. Analysis of non-stationary temperature distributions inside of solid particles of characteristic size $r_0 \sim 1$–$10\ \mu$m, including those of non-uniform q_0, also confirms the validity of this approximation [9, 10]. Moreover, on solid particle melting a thermocapillary circulation may arise which leads to an additional equalization of temperatures inside of the particle. After integration over the volume for the spherically symmetric case and transition to a uniform temperature T_0 and also after the introduction of the mass balance equation for the particle, the system of equations which describes the heating and evaporation of a particle and which results from equation (1) will have the form [1]

$$\rho_0V_0C_0\frac{\mathrm{d}T_0}{\mathrm{d}t} = \tfrac{1}{4}I_0(t)K_{ab}S_0-\bar{j}_\varepsilon S_0 \quad (4)$$

$$\frac{\mathrm{d}(\rho_0V_0)}{\mathrm{d}t} = -\bar{j}S_0 \quad (5)$$

with the initial conditions

$$T_0(t=0) = T_\infty, \quad r_0(t=0) = r_\infty \quad (6)$$

where

$$\int_0^{r_0} q_0(t)4\pi r^2\,\mathrm{d}r = 1/4I_0(t)K_{ab}S_0$$

and $\bar{j}$ is the density of the mass flux removed from the particle surface. Equations (4) and (5) take into account phase changes that occur during heating and cooling of the particle. In the general case, the quantity $\bar{j}_\varepsilon$ near the particle surface is composed of energy losses due to hydrodynamic energy transfer, evaporation $\bar{j}_{ev}$, heat conduction $\bar{j}_{cond}$, radiation cooling $\bar{j}_{rad}$ and energy generation due to chemical reaction

$$\bar{j}_\varepsilon = \bar{j}C_p\bar{T}+\bar{j}_{ev}+\bar{j}_{cond}+\bar{j}_{rad}+q_{ch}\bar{j}_3. \quad (7)$$

Of great interest is the study of the integral energy parameters that characterize the interaction of radiation with the particle—its heating, evaporation, combustion, etc., from the onset of irradiation $t = 0$ to the time considered t; the quantities of radiation energy absorbed Q_{ab} by, and scattered Q_{sc}, from the particle; the quantities of heat spent for particle evaporation Q_{ev} and removed from the particle by heat conduction Q_{cond}; the quantities of heat removed from the particle surface by thermal radiation Q_{rad} and generated on the particle surface due to heterogeneous chemical reaction Q_{ch}, and also the thermal energy of the particle E_T and the energy spent for particle melting Q_m

$$Q_{ab} = \pi\int_0^t I_0(t)K_{ab}(r_0, T_0)r_0^2\,\mathrm{d}t$$

$$Q_{sc} = \pi\int_0^t I_0(t)K_{sc}(r_0, T_0)r_0^2\,\mathrm{d}t$$

$$Q_{ev} = 4\pi\int_0^t \bar{j}_{ev}r_0^2\,\mathrm{d}t$$

$$Q_{cond} = 4\pi\int_0^t \bar{j}_{cond}r_0^2\,\mathrm{d}t$$

$$Q_{rad} = 4\pi\int_0^t \bar{j}_{rad}r_0^2\,\mathrm{d}t$$

$$Q_{ch} = -4\pi\int_0^t \bar{q}_{ch}\bar{j}_3r_0^2\,\mathrm{d}t$$

$$E_T = C_0\rho_0V_0T_0, \quad Q_m = \rho_0V_0L_m \quad (8)$$

where

$$\bar{j}_{rad} = \varepsilon\sigma(T_0^4-T_\infty^4), \quad \bar{j}_{cond} = -\kappa\left.\frac{\mathrm{d}T}{\mathrm{d}r}\right|_{r=r_0}.$$

Consider also the energy parameters M_i that characterize the contribution of separate processes into the general energy balance of the particle

$$M_1 = \frac{Q_{ev}}{Q_{ev}+Q_{cond}+Q_{rad}}; \quad M_2 = \frac{Q_{ev}}{Q_{ab}+Q_{sc}};$$
$$M_3 = \frac{Q_{ab}}{Q_{ab}+Q_{sc}}; \quad M_4 = \frac{Q_{cond}}{Q_{ev}+Q_{cond}+Q_{rad}};$$
$$M_5 = \frac{Q_{rad}}{Q_{ev}+Q_{cond}+Q_{rad}}; \quad M_6 = \frac{Q_{ch}}{Q_{ab}+Q_{ch}}. \qquad (9)$$

2.1. *Temperature dependence of the optical parameters of material*

When a particle is heated by radiation, it is important to take into account the temperature dependence of the optical parameters of the particle material, i.e. the dependence of the indices of refraction n_λ, and absorption κ_λ for the particle material at the wavelength λ on the particle temperature. Unfortunately, at present there are no systematic data on the temperature dependence of $n_\lambda, \kappa_\lambda$ for a wide class of materials [13]. At the same time, there are rather detailed data for some of the materials. As an example, consider the effect of the temperature dependence of $n_\lambda, \kappa_\lambda$ on the factor K_{ab} of an Al_2O_3 particle. The particles of Al_2O_3 are of interest because they are often met in modern power engineering and plasma-technological equipment, in the atmospheric aerosol, etc. The data on K_{ab} of spherical Al_2O_3 particles for the ranges $0.1 \leqslant r_0 \leqslant 10\ \mu m$ and $1493 \leqslant T_0 \leqslant 2293$ K are given in ref. [14]. However, the data presented in ref. [14] are quite inadequate at present, since they were obtained for relatively narrow ranges of variation of r_0 and T_0 and are virtually of no importance because of the inconsistency between the values of $n_\lambda, \kappa_\lambda$ used for calculations in ref. [14] and those values of n_λ, which were found in recent publications [15, 16]. In what follows, the factor K_{ab} of Al_2O_3 spherical particles will be given for radiation at a wavelength of 1.06 μm for particles with radii in the range $0.1 \leqslant r_0 \leqslant 40\ \mu m$ and temperatures in the range $300 \leqslant T_0 \leqslant 2800$ K. For the temperature range $300 \leqslant T_0 \leqslant 2300$ K the values of n_λ and κ_λ were determined by means of linear interpolation of the data of ref. [15], and for the range $2400 \leqslant T_0 \leqslant 2800$ K the values of $n_\lambda, \kappa_\lambda$ were borrowed from ref. [16]. For example, for $T_0 = 300, 900, 1700, 2300, 2403, 2800$ K the values of $n_\lambda, \kappa_\lambda$ are respectively equal to

$$n_\lambda = 1.755, 1.770, 1.791, 1.809, 1.809, 1.829;$$
$$\kappa_\lambda = 2.06\times10^{-8}, 5.48\times10^{-8}, 1.92\times10^{-7}, 2.01\times10^{-6}, 5.90\times10^{-5}, 5.70\times10^{-4}.$$

Numerical calculations of K_{ab} were carried out by the technique of refs. [17, 18] with the step over the particle radius of 0.1 μm. The dependence of K_{ab} on r_0 for $\lambda = 1.06\ \mu m$ and several values of T_0 [19] are given in Fig. 1(a). The absorption factor K_{ab} increases with r_0 undergoing specific oscillations due to resonance effects. An increase of T_0 from 300 to 2800 K leads to an increase of K_{ab} for a fixed r_0 up to $\sim 10^5$.

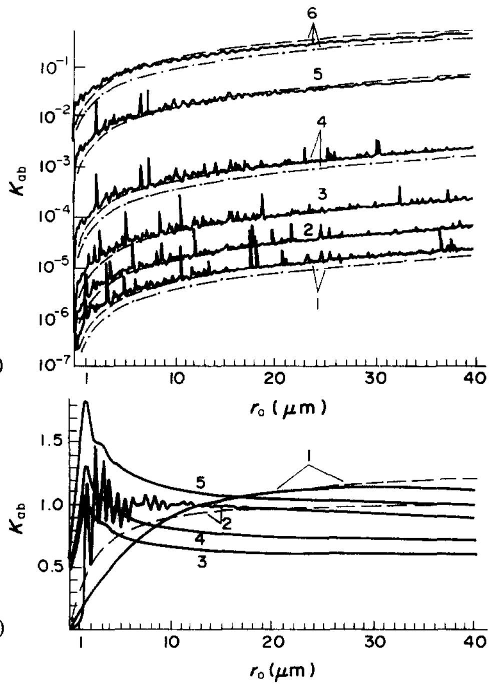

FIG. 1. Dependence of the factor K_{ab} on r_0 for Al_2O_3 particles at $T_0 = 300$ (1), 900 (2), 1700 (3), 2300 (4), 2403 (5), 2800 (6) K and $\lambda = 1.06\ \mu m$ (a); for water [23] (1) and boron (2) particles at $T_0 = 300$ K; for aluminium at $T_0 = 300$ (3), 922.5 (4), 944.7 (5) K and $\lambda = 10.6\ \mu m$ (b). Solid curve, calculation by the Mie theory; dashed curve, approximation (10); dashed curve, approximation of ref. [20].

The value of K_{ab} increases most considerably (up to about 10^2) on an increase of T_0 from 2300 to 2403 K, i.e. during the transition of a particle into a melted state. All this should lead to a non-linear dependence of heat generation in a particle on the optical radiation energy absorption, especially near T_m. Note that detailed data for the efficiency factors for absorption, K_{ab}, extinction and scattering, K_{sc}, of radiation with $\lambda = 0.63$ and 1.06 μm by spherical Al_2O_3 particles with $0.1 \leqslant r_0 \leqslant 40\ \mu m$ and $300 \leqslant T_0 \leqslant 2800$ K can be found in ref. [19].

Of great interest is the use of an approximating formula for the effectiveness factor K_{ab} to describe the dependence of K_{ab} on r_0, λ and T_0 [1]

$$K_{ab} = K_1 r_0 \left[1-\exp\left(-\frac{K_2}{r_0}\right)\right] \qquad (10)$$

where K_1, K_2 are some functions of n_λ, κ_λ, λ. In the present case, when $\kappa_\lambda \ll 1$ and $n_\lambda \approx$ const., it is possible to assume that $K_1 = K_2^{-1} = 8\pi\kappa_\lambda/\lambda$. Figure 1 presents the functions $K_{ab}(r_0)$, equation (10), with the values of K_1 and K_2 for corresponding T_0 and κ_λ. It follows from Fig. 1 that equation (10) with the indicated values of K_1 and K_2 rather well (with an error $\leqslant 20\%$) describes the behaviour of the function $K_{ab}(r_0, T_0)$, averaging also the resonance oscillations. The well-known analytical approximation for K_{ab} [20] (Fig. 1) admits a much higher mean error; moreover, for small r_0's this approximation may disagree with the predicted values of K_{ab} by almost an order of magnitude. Consequently, equation (10) gives a better description of the function $K_{ab}(r_0, \kappa_\lambda, \lambda)$ than the approximating formula of ref. [20].

2.2. *Diffusive–convective heat and mass transfer*

The treatment of evaporation or combustion of a particle within the temperature range $T_\infty < T_0 \lessgtr T_b$ when the pressure of the particle material saturated vapour or of gaseous reaction products become comparable with surrounding gas pressure, when $T_0 \leqslant T_b$, requires that the convective (hydrodynamic) heat and mass transfer in the medium be taken into account. At the same time, within the temperature range $T_\infty < T_0 \leqslant T_m$ the convective heat and mass transfer is small, and the main part is played here by diffusion and heat conduction. Consequently, diffusive–convective heat and mass transfer for a spherically-symmetric case will be considered provided that there is a uniform and constant gas pressure throughout the entire volume, since mass velocities originating during convection are much smaller than the speed of sound in a gas. In this case, the heat and mass transfer processes will be considered in a quasi-steady-state approximation, since estimates indicate that characteristic times required for the processes of heat conduction $t_{cond} \sim r_0^2/\psi$, diffusion $t_d \sim r_0^2/D$ and convection $t_c \sim r_0/v$ to be developed are much smaller than the characteristic times of heating, evaporation, and combustion of a particle. The system of equations that describes the processes of quasi-steady-state diffusive–convective heat and mass transfer in the gas surrounding the particle, with thermal diffusion and heat transfer by diffusion being neglected, has the following form in a spherical coordinate system:

$$\frac{1}{r^2}\frac{d}{dr}(r^2\rho v) = 0 \tag{11}$$

$$\frac{1}{r^2}\frac{d}{dr}\left[r^2\left(\rho v c_i - \rho D\frac{dc_i}{dr}\right)\right] = 0 \tag{12}$$

$$p = R_g\rho T = p_\infty = \text{const.} \tag{13}$$

$$\rho v C_p\frac{dT}{dr} = \frac{1}{r^2}\frac{d}{dr}\left(r^2\kappa\frac{dT}{dr}\right) \tag{14}$$

with boundary conditions

$$r = r_0: \quad \rho = \bar\rho, \quad v = \bar v, \quad T = \bar T, \quad c_i = \bar c_i, \quad j_i = \bar j_i \tag{15}$$

$$r \to \infty: \quad \rho = \rho_\infty, \quad v = 0, \quad T = T_\infty, \quad c_i = c_{i\infty}, \quad j_i = 0 \tag{16}$$

where $c_i = \rho_i/\rho$ is the concentration of the ith component

$$i = 1,2,3,4; \quad \sum_i \rho_i = \rho; \quad \sum_i c_i = 1;$$

$j_i = \rho v c_i - \rho D(dc_i/dr)$ is the mass flux density of the ith component; the coefficients of interdiffusion of different components in the mixture are assumed to be the same and equal to D; $\sum_i j_i = j$. Equations (12) and (14) describe the diffusion of gas components in the medium and heat transfer with regard for convection; equation (11) is the continuity equation; equation (13) represents the condition for pressure constancy in the medium. Integration of equations (11) and (12) with the use of equation (15) will yield

$$\frac{r^2 p_\infty}{R_g T}D\frac{dc_i}{dr} = r_0^2\bar j(c_i - A_i) \tag{17}$$

where A_i = const. and it is determined from equations (15) and (16). Assuming R_g = const., C_p = const., equation (14), taking into account equation (13), will give

$$r^2\kappa\frac{dT}{dr} = r_0^2\bar j(T-B)C_p \tag{18}$$

where the integration constant B is determined from equations (15) and (16). When κ depends only on T, $\kappa(T)$, equation (14), taking into account equations (13) and (11), will yield

$$\int\frac{\kappa(T)}{T-B}dT = -\frac{r_0^2\bar j C_p}{r} + F \tag{19}$$

where the integration constant F is determined from equations (15) and (16). Equation (19) represents the temperature distribution $T(r)$ at an arbitrary function $\kappa(T)$. In particular, the coefficients of thermal conductivity κ and diffusion D can be represented with a good accuracy within a wide temperature range in the form of the power functions of temperature [6]

$$\kappa = \kappa_\infty\left(\frac{T}{T_\infty}\right)^a, \quad D = D_\infty\left(\frac{T}{T_\infty}\right)^b \tag{20}$$

where $\kappa_\infty = \kappa(T_\infty)$; $D_\infty = D(T_\infty)$; a, b = const. $\geqslant 0$ for gaseous media. For $\kappa(T)$ (equation (20)) and for practically the most important range $0 \leqslant a \leqslant 1$ [6] the following solutions [21] can be obtained from equation (19) taking into account equations (15) and (16):

$$a = 0, \quad T = T_\infty + \frac{\bar T - T_\infty}{1-\exp(-r_0\bar j C_p/\kappa_\infty)} \times\left[1-\exp\left(-\frac{r_0^2\bar j C_p}{\kappa_\infty r}\right)\right];$$

$$a = \tfrac{1}{2}, \quad T^{1/2} - T_\infty^{1/2} + \frac{B^{1/2}}{2} \times\ln\frac{(B^{1/2}-T^{1/2})(B^{1/2}+T_\infty^{1/2})}{(B^{1/2}+T^{1/2})(B^{1/2}-T_\infty^{1/2})} = -\frac{T_\infty^{1/2}r_0^2\bar j C_p}{2\kappa_\infty r};$$

$$a = \tfrac{2}{3}, \quad \tfrac{3}{2}(T^{2/3} - T_\infty^{2/3}) + \sqrt{3}\,B^{2/3}\left(\arctan\frac{2T^{1/3}+B^{1/3}}{\sqrt{3}\,B^{1/3}}\right.$$

$$-\arctan\frac{2T_\infty^{1/3}+B^{1/3}}{\sqrt{3}B^{1/3}}\bigg)-\frac{B^{2/3}}{2}$$

$$\times\ln\frac{(B^{2/3}+B^{1/3}T^{1/3}+T^{2/3})(B^{1/3}-T_\infty^{1/3})}{(B^{1/3}-T^{1/3})^2(B^{2/3}+B^{1/3}T_\infty^{1/3}+T_\infty^{2/3})}$$

$$=-\frac{T_\infty^{2/3}r_0^2\bar{j}C_p}{\kappa_\infty r};$$

$$a=\tfrac{3}{4},\quad \tfrac{4}{3}(T^{3/4}-T_\infty^{3/4})+2B^{3/4}$$

$$\times\left(\arctan\frac{T^{1/4}}{B^{1/4}}-\arctan\frac{T_\infty^{1/4}}{B^{1/4}}\right)$$

$$+B^{3/4}\ln\frac{(B^{1/4}+T_\infty^{1/4})(B^{1/4}-T^{1/4})}{(B^{1/4}-T_\infty^{1/4})(B^{1/4}+T^{1/4})}$$

$$=-\frac{T_\infty^{3/4}r_0^2\bar{j}C_p}{\kappa_\infty r};$$

$$a=1,\quad T-T_\infty+B\ln\frac{T-B}{T_\infty-B}=-\frac{T_\infty r_0^2\bar{j}C_p}{\kappa_\infty r}. \tag{21}$$

At $r=r_0$, equations (21) may give expressions for $\bar{j}$, such as for example

$$a=\tfrac{3}{4},\quad \bar{j}=\frac{\kappa_\infty}{C_pT_\infty^{3/4}r_0}$$

$$\times\left[B^{3/4}\ln\frac{(B^{1/4}+\bar{T}^{1/4})(B^{1/4}-T_\infty^{1/4})}{(B^{1/4}-\bar{T}^{1/4})(B^{1/4}+T_\infty^{1/4})}\right.$$

$$-\tfrac{4}{3}(\bar{T}^{3/4}-T_\infty^{3/4})-2B^{3/4}$$

$$\left.\times\left(\arctan\frac{\bar{T}^{1/4}}{B^{1/4}}-\arctan\frac{T_\infty^{1/4}}{B^{1/4}}\right)\right]. \tag{22}$$

Neglecting convection at $v=0$, equations (11)–(14), taking into account equations (15), (16) and (20), yield the following solutions:

$$T=T_\infty\left[1+\frac{r_0}{r}(\bar{T}_n^{a+1}-1)\right]^{1/(a+1)}$$

$$\bar{j}_{\text{cond}}=-\kappa\frac{\mathrm{d}T}{\mathrm{d}r}\bigg|_{r_0}=\frac{\kappa_\infty T_\infty}{(a+1)r_0}[\bar{T}_n^{a+1}-1]; \tag{23}$$

when $a\neq b-2$

$$c_i=c_{i\infty}+(\bar{c}_i-c_{i\infty})$$

$$\times\frac{\left\{1-\left[1+\frac{r_0}{r}(\bar{T}_n^{a+1}-1)\right]^{(a-b+2)/(a+1)}\right\}}{(1-\bar{T}_n^{a-b+2})}$$

$$\bar{j}_i=-\rho D\frac{\mathrm{d}c_i}{\mathrm{d}r}\bigg|_{r_0}$$

$$=\frac{\rho_\infty D_\infty(\bar{c}_i-c_{i\infty})(a-b+2)}{r_0(a+1)(\bar{T}_n^{a-b+2}-1)}(\bar{T}_n^{a+1}-1); \tag{24}$$

when $a=b-2$

$$c_i=c_{i\infty}+(\bar{c}_i-c_{i\infty})\frac{\ln\left[1+\frac{r_0}{r}(\bar{T}_n^{a+1}-1)\right]}{(a+1)\ln\bar{T}_n}$$

$$\bar{j}_i=-\rho D\frac{\mathrm{d}c_i}{\mathrm{d}r}\bigg|_{r_0}=\frac{\rho_\infty D_\infty(\bar{c}_i-c_{i\infty})(\bar{T}_n^{a+1}-1)}{r_0(a+1)\ln\bar{T}_n} \tag{25}$$

where $\bar{T}_n=\bar{T}/T_\infty$. Note that expressions (23) were earlier obtained in ref. [1]. The expansion of equations (21) in the small parameters $r_0\bar{j}C_p/\kappa_\infty$ (for $a=0$) and T/B, T_∞/B (for $1/2\leqslant a\leqslant 1$) leads to equations (23). The expansion of the $\bar{j}$'s, obtainable from equations (21) (e.g. equation (22)), in small parameters $\bar{c}_i$, $c_{i\infty}$ (see equation (29)) results in expressions (24) and (25). Thus, the expressions for T (equations (21)) and $\bar{j}$ (e.g. equation (22)) obtained with convective motion taken into account, admit the limiting transition to expressions (23)–(25) for the diffusional mode of heat and mass transfer. Equation (17) can be integrated, with regard to equations (20), in the form

$$\ln\left|\frac{c_{i\infty}-A_i}{c_i-A_i}\right|=\frac{r_0^2\bar{j}R_gT_\infty^b}{p_\infty D_\infty}\int_r^\infty\frac{T(r)^{1-b}\,\mathrm{d}r}{r^2}. \tag{26}$$

On the substitution $T(r)$, equation (26) yields the distribution $c_i(r)$. For example, when $b=1$, equation (26) gives

$$c_i=A_i+|c_{i\infty}-A_i|\exp\left(\frac{r_0}{r}\ln\left|\frac{\bar{c}_i-A_i}{c_{i\infty}-A_i}\right|\right).$$

The combination of equations (17) and (18) results in the following equation which relates c_i and T:

$$\ln\left|\frac{c_i-A_i}{\bar{c}_i-A_i}\right|=\frac{R_g\kappa_\infty T_\infty^{b-a}}{p_\infty C_pD_\infty}\int_{\bar{T}}^{T(r)}\frac{T^{a-b+1}}{T-B}\mathrm{d}T. \tag{27}$$

For example, when $a=b=0$, equation (27) has the following solution:

$$\ln\left|\frac{c_i-A_i}{\bar{c}_i-A_i}\right|=\frac{R_g\kappa_\infty}{p_\infty C_pD_\infty}\left(T-\bar{T}+B\ln\left|\frac{B-T}{B-\bar{T}}\right|\right).$$

One of the practically most important cases is that with $a=b-1$, since exponents a and b usually lie within the limits $1/2<a<1$ and $3/2<b<2$ [6]. In this case equation (27) gives

$$c_i=A_i+(\bar{c}_i-A_i)\left(\frac{B-T}{B-\bar{T}}\right)^{1/d} \tag{28}$$

where $d=p_\infty C_pD_\infty/R_g\kappa_\infty T_\infty$. With the aid of equations (15) and (16), equation (28) determines the quantity B

$$B=\frac{\left|\bar{T}\left(\frac{A_i-c_{i\infty}}{A_i-\bar{c}_i}\right)^d-T_\infty\right|}{\left|\left(\frac{A_i-c_{i\infty}}{A_i-\bar{c}_i}\right)^d-1\right|}. \tag{29}$$

Thus, equations (21) and (22), with equations (7), (15), (16) and (29) taken into account, make it possible to determine the densities of the resulting mass $\bar{j}$ and energy $\bar{j}_\varepsilon$ fluxes directly near the particle surface in the case of diffusive–convective heat and mass transfer with regard for the temperature dependence of the coefficients κ and D, equations (20).

3. HEATING AND EVAPORATION OF AN AEROSOL PARTICLE IN AN INERT GAS

Now, consider the heating and evaporation of an aerosol particle in an inert gas under the action of intense optical radiation. In this case the gas does not react with the vapours of the particle material and its surface and, therefore, $q_{ch}\bar{j}_3$ in equation (7) is assumed to be equal to zero. The gas medium surrounding the particle in the process of its evaporation is a two-component mixture consisting of the particle material vapours and inert gas and having

$$\rho = \rho_1 + \rho_2, \quad c_1 + c_2 = 1. \tag{30}$$

Boundary conditions (15) and (16) in this case should be augmented with the relations:

for $r = r_0$

$$\bar{j}_1 = \alpha_0 \left[\rho_{0\mathrm{sat}} \left(\frac{kT_0}{2\pi m_0} \right)^{1/2} - \bar{c}_1 \bar{\rho} \left(\frac{k\bar{T}}{2\pi m_0} \right)^{1/2} \right],$$

$$\bar{j}_2 = 0, \quad \bar{j}_{\mathrm{ev}} = \bar{j}_1 L_0 \tag{31}$$

the first of which describes the kinetics of particle material evaporation [1] and the second signifies the zero gas flow at the particle boundary. Since the mass velocity of vapour removal v is much smaller than the local speed of sound in the gas, the temperature jumps near the particle surface will be small $T_0 - \bar{T} \ll T_0$ and it is possible to assume that $T_0 = \bar{T}$ in equations (31). With regard for equations (30) and (31) and $T_0 = \bar{T}$, expression (29) for B at $a = b - 1$ becomes

$$B = \left| T_0 \left(\frac{1 - \bar{c}_1}{1 - c_{1\infty}} \right)^{-d} - T_\infty \right| \Big/ \left| \left(\frac{1 - \bar{c}_1}{1 - c_{1\infty}} \right)^{-d} - 1 \right|. \tag{32}$$

The system of equations that describe the process of heating and evaporation of a particle in an inert gas incorporate equations (4) and (5) with initial, equation (6), and boundary, equations (15), (16) and (31), conditions with equation (7) taken into account at $q_{ch}\bar{j}_3 = 0$, equations (18), (21), (22) and (32).

3.1. *Comparison with experimental data*

To check the theory, calculations were made for water droplets evaporating in air at atmospheric pressure in a diffusive–convective regime on exposure to continuous optical radiation with $\lambda = 10.6$ μm, and the results of calculations were compared with the experimental data of ref. [22]. The water evaporation (condensation) coefficient α_0 was assumed equal to 1. The function $K_{ab}(r_0)$ for a water droplet at $\lambda = 10.6$ μm is represented by relation (10) with $K_1 = 1.38 \times 10^3$ cm^{-1}, $K_2 = 9.8 \times 10^{-4}$ cm, which approximates $K_{ab}(r_0)$ [23] with a mean error of less than 10% for the range $0.1 < r_0 < 40$ μm (Fig. 1). Expression (20) for $D(T)$ with $D_\infty = 2.16 \times 10^{-5}$ m^2 s^{-1}, $b = 1.75$ [6] has a mean error of no more than 5% within the temperature range $273 < T < 493$ K. The temperature function $\kappa(T)$ [6] is approximated by relation (20) at $\kappa_\infty = 2.4 \times 10^{-2}$ W m^{-1} K^{-1}, $a = 0.75$ within the temperature range $273 < T < 473$ K. The values of the rest parameters are borrowed from refs. [1, 2, 6]. The temperature jump $T_0 - \bar{T}$ at the boundary of an evaporating water droplet with $r_\infty = 5$–40 μm does not exceed 1–4 K [1], thus confirming the validity of the use of the condition $T_0 = \bar{T}$. The vapour density jump on the droplet boundary is taken into account on the basis of the kinetic description of the processes of evaporation and condensation, equations (31). In our case $a = 0.75$, $b = 1.75$ and $a = b - 1$. Consequently, equations (22) will be used for $\bar{j}$ and equation (29) for B.

Numerical calculations were made for water droplets with $r_\infty = 15, 25$ and 35 μm at $I_0 = 0.93$ kW cm^{-2} and with $r_\infty = 6$ μm at $I_0 = 13$ kW cm^{-2} to compare with experimental data of ref. [22]. Figure 2 presents the experimental and predicted functions $r_0(t)$ and $T_0(t)$. The predicted functions $r_0(t)$ are in good agreement with experimental results, thus confirming the correctness of the approximations employed. It should be noted that in the process of heating and evaporation the maximum temperature of the droplet with $r_\infty = 6$ μm somewhat exceeds (by about 4 K) the value $T_b = 373$ K. However, the vapour density jump at the evaporating droplet surface being taken into account, equations (31), leads to the situation that the vapour pressure does not exceed the atmospheric pressure and the use of the diffusive–convective regime

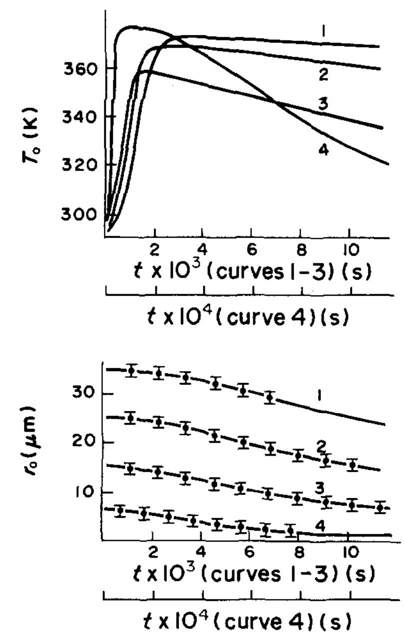

FIG. 2. Temperature T_0 and radius r_0 of a water droplet vs time t at $r_\infty = 35$ (1), 25 (2), 15 (3) μm, $I_0 = 0.93$ kW cm^{-2} and at $r_\infty = 6$ μm, $I_0 = 13$ kW cm^{-2} (4). Dots, experimental data of ref. [22]; vertical segments, experimental error.

of droplet evaporation at $p = \text{const.}$ is justifiable. Upon the attainment of the maximum temperature, T_0 decreases in the process of droplet evaporation.

3.2. *Heating and evaporation of a solid aerosol particle in an inert gas*

The interaction of intense radiation with a solid (metallic) particle in an inert gas is of interest for the problems depositing powder materials substrates by the action of intense radiation.

Consider heating, melting and evaporation of a spherical aluminium particle with r_∞ in helium at an atmospheric pressure p_∞ on exposure to optical radiation with I_0 and $\lambda = 10.6\ \mu\text{m}$. In this case, boundary conditions (16), taking into account equations (30), will acquire the form

$$r = \infty: \quad \rho = \rho_\infty, \quad T = T_\infty, \quad v = 0, \quad c_{1\infty} = 0,$$
$$c_{2\infty} = 1, \quad j_i = 0. \quad (33)$$

With the above equations taken into account, equation (32) for B will become

$$B = \left| \frac{T_0(1-\bar{c}_i)^{-d} - T_\infty}{(1-\bar{c}_i)^{-d} - 1} \right|. \quad (34)$$

The thermophysical parameters of aluminium and helium are borrowed from refs. [2, 6, 28]. The thermal conductivity coefficient of helium within the temperature range $300 < T < 3000$ K is approximated by the function $\kappa(T)$, equations (20), at $\kappa_\infty = 1.45 \times 10^{-1}$ W m^{-1} K^{-1}, $a = 0.75$ with a mean error of less than 5% [6]. The temperature dependence of the diffusion coefficient for aluminium atoms in helium is approximated, at $b = 1.75$ and $D_\infty = 6.22 \times 10^{-5}$ m^2 s^{-1}, by the function $D(T)$, equations (20), obtained on the basis of the molecular–kinetic theory. The effectiveness factors K_{ab} and K_{sc} for spherical aluminium particles irradiated at $\lambda = 10.6\ \mu$m were calculated by Mie theory, with the temperature dependence of the indices of refraction n_λ and absorption κ_λ of aluminium [24] taken into account. At $T_0 = T_\infty$, it was assumed that $n_\lambda = 36$, $\kappa_\lambda = 45$. When $T_\infty < T_0 < T_m$, the normal skin effect theory was employed; when $T_0 \geqslant T_m$, it was adopted that $n_\lambda = 24.8$ and $\kappa_\lambda = 27$. Figure 1(b) presents the calculated K_{ab} of aluminium particles for several values of T_0. In this case, when n_λ, $\kappa_\lambda \gg 1$, the use of equation (10) for K_{ab} leads to considerable errors. Figure 3 presents the plots for T_0 and dimensionless radius $r_n = r_0/r_\infty$ of aluminium particles with $r_\infty = 2.5$, 10, 25 μm and $T_\infty = 300$ K heated and evaporating on exposure to radiation with $I_0 = 0.1$, 0.5 and 1 MW cm^{-2}. From the instant of particle irradiation, radiation energy absorption and rapid growth of T_0 begin. Upon the attainment of the melting temperature T_m, the particle is being melted for a certain period of time Δt_m. Before and during particle melting, there is virtually no evaporation, and the heat is removed from the particle by the mechanisms of heat conduction and radiation cooling with

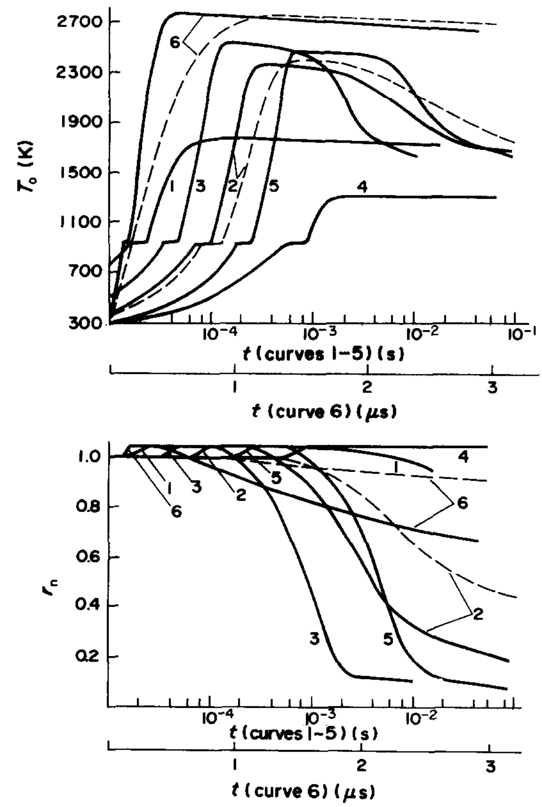

FIG. 3. Temperature T_0 and dimensionless radius $r_n = r_0/r_\infty$ of aluminium particles vs time t at $r_\infty = 2.5$ (1), 10 (2–4), 25 (5) μm at $I_0 = 0.1$ (4), 0.5 (1, 2, 5), 1 (3) MW cm^{-2} (6) and with $r_0 = 0.25\ \mu$m, $I_0 = 10$ MW cm^{-2} (6). Solid curve, calculations from equations (4)–(7), (22), (33), (34); dashed curve, results borrowed from ref. [5] and calculation by the technique of refs. [4, 5].

the energy fluxes $\bar{j}_{cond}$ and $\bar{j}_{rad}$. The interval Δt_m can be estimated by (see equation (4))

$$\Delta t_m = \frac{4 r_\infty \rho_{0s} L_m}{3(I_0 K_{ab} - 4\bar{j}_{cond} - 4\bar{j}_{rad})}. \quad (35)$$

In many cases it is possible to neglect $\bar{j}_{cond}$ and $\bar{j}_{rad}$ in equation (35) as compared with $I_0 K_{ab}$, and Δt_m can be estimated from

$$\Delta t_m = \frac{4 r_\infty \rho_{0s} L_m}{3 I_0 K_{ab}(T_m, r_\infty)}. \quad (36)$$

For example, for $r_\infty = 10\ \mu$m at $I_0 = 0.1$, 0.5, 1 MW cm^{-2} equation (36) can respectively yield: $\Delta t_m \times 10^5 = 14$, 2.8, 1.4 s, in accord with the predicted results (Fig. 3). On melting or solidification of the particle in the process of heating and cooling, such parameters as ρ_0, C_0, κ_0, n_λ, κ_λ, and also the radius r_0 and volume V_0, undergo substantial variations. When $T_0 < T_m$ and $T_0 \geqslant T_m$, the parameters for a solid or liquid state of the particle material will be respectively used in equations. An interesting effect occurring during particle melting should be noted (Fig. 3). The density of aluminium in transition from the solid to the liquid state decreases noticeably: from

$\rho_0 = 2.7 \times 10^3$ kg m^{-3} to $\rho_{0l} = 2.35 \times 10^3$ kg m^{-3} [2]. In the absence of perceptible evaporation, this leads to an increase in the particle radius after melting according to the particle mass conservation law

$$r_{0s}^3 \rho_{0s} = r_{0l}^3 \rho_{0l}, \quad r_{0l} = r_{0s}\left(\frac{\rho_{0s}}{\rho_{0l}}\right)^{1/3} \tag{37}$$

with $r_{0l} = 1.05 r_{0s}$ for aluminium. Inclusion into calculations of the varying constants of melting aluminium leads for $r_\infty = 10$ μm to an increase of $K_{ab} = 8.27 \times 10^{-2}$ at $T_0 = 922.5$ K, T_m up to the value $K_{ab} = 1.13 \times 10^{-1}$ when $T_0 \geqslant T_m$ (Fig. 1). The above all leads to a noticeable increase in the coefficient of radiation absorption by a particle $\pi r_0^2 K_{ab}$ in melting (by about a factor of 1.5) and, in turn, to higher energy generation and a more rapid particle heating. This can be seen from Fig. 3 from a change in the slope of the curves $T_0(t)$ when $T_0 > T_m$. This effect accompanies the heating and melting of particles of many materials on exposure to optical radiation, with even greater variation of r_0 [2] than in the case considered. The reverse takes place on particle solidification as T_0 decreases in the radiation field.

After the particle was melted, an increase of T_0 leads to an increase of heat losses due to evaporation and heat conduction. The rate of particle material evaporation depends drastically (see equation (31)) $\rho_{0sat} \sim \exp(-1/T_0)$, on T_0, therefore the heating (or cooling) of an aluminium particle below $T_0 \sim 1500$–1700 K does not virtually cause (or cease) its evaporation, and the energy generated in the particle is carried away by the mechanisms of non-linear heat conduction and radiative cooling. At the same time, the heating of the particle above $T_0 \sim 1700$ K leads to an appreciably more rapid evaporation and to greater energy losses by the particle. Since the evaporation rate depends strongly on T_0, it is possible to say that evaporation of a solid particle by the action of radiation is a threshold phenomenon. At a certain time instant t_{max} the energy generation in a particle due to radiation energy absorption and the energy losses due to evaporation, heat conduction and radiative cooling balance out and the particle temperature attains the maximum value T_{max}. For example, at $r_\infty = 10$ μm and $I_0 = 0.5$ MW cm^{-2}, $t_{max} = 3.4 \times 10^{-4}$ s, $T_{max} = 2370$ K. After the attainment of T_{max} when $t > t_{max}$, T_0 of the particle begins to decrease in the process of particle evaporation. The effect of particle radius increase during particle melting leads to a situation when the relative radius of the evaporating particle $r_n = r_0/r_\infty$ becomes smaller than 1 some time after the attainment of T_{max}. The parameters and dynamics of solid particle evaporation on exposure to optical radiation depend substantially on I_0, r_∞ and on the particle material characteristics. An increase of I_0 at r_∞ = const. leads to a smaller time needed for the particle to be heated up to T_m and to a smaller Δt_m to a higher T_{max}, and to a more rapid particle evaporation (Fig. 3), and conversely. An increase of r_∞ at I_0 = const. leads to an increase in the time of heating up to T_m, Δt_m, to a higher T_{max} and to a substantially more rapid particle evaporation. The effect of T_∞ within the range $300 < T_\infty < 500$ K on solid particle evaporation is small. Figure 3 presents the results of calculations for $r_\infty = 0.25$ μm and $I_0 = 10$ MW cm^{-2} which were borrowed from ref. [5] and which were calculated from equations (4)–(7), (22), (33) and (34) with the constants of ref. [5], and also the results of calculations at $r_\infty = 10$ μm, $I_0 = 0.5$ MW cm^{-2} carried out by the technique of refs. [4, 5]. It should be noted that at $r_\infty = 0.25$ μm and $T_0 = T_{max}$ the aluminium vapour pressure near the particle surface is smaller than that of the surrounding gas [2, 28]. A marked underestimation of the particle evaporation rate in the versions calculated by the technique of refs. [4, 5] seems to be due to the disregard of convective heat and mass transfer, actual temperature dependencies of optical and thermophysical parameters and of transfer coefficients.

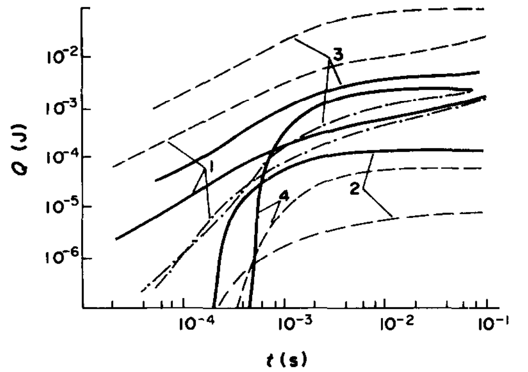

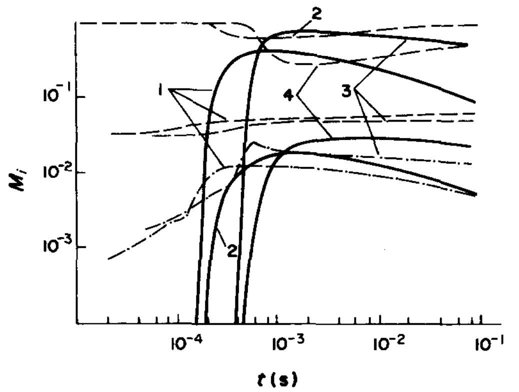

FIG. 4. The energies Q_{ab} (1, 3), Q_{ev} (2, 4)—solid lines, Q_{sc} (1, 3), Q_{rad} (2, 4)—dashed lines, Q_{cond} (1,3)—dashed-dotted lines (a) and the parameters M_1 (1, 3), M_2 (2, 4)—solid lines, M_3 (1, 3), M_4 (2, 4)—dashed lines (b) vs time t for aluminium particles with $r_\infty = 10$ (1, 2), 25 (3, 4) μm at $I_0 = 0.5$ MW cm^{-2}.

Figure 4 shows the time dependence of the energies Q_{ab}, Q_{sc}, Q_{ev}, Q_{cond}, Q_{rad} and of the parameters M_i that characterize the contribution of separate processes into the overall energy balance of the particle. At $r_\infty = 10$, 25 μm, an intensive evaporation of a particle takes place during which the energies Q increase monotonously. When $r_n < 0.1$, the energies attain their stationary values. In this case, the absorption and scattering of radiation energy by a particle slow down appreciably, the energy Q_{ab} is almost completely vented away by heat conduction and radiative cooling. The parameters M_1 and M_2 depend considerably on r_∞ and t, whereas M_3 depends weakly on r_∞ and t. A simple estimation of M_3 can be obtained by employing the following relation [1]:

$$M_3 = \frac{K_{ab}}{K_{ab}+K_{sc}}. \tag{38}$$

In the present case, for $r_\infty = 10$, 25 μm equation (38) yields $M_3 \approx 5.21\times10^{-2}$; 4.89×10^{-2}, in good agreement with the data predicted. Relations given in Fig. 4 show the effect of r_∞ on the process characteristics.

Having integrated equation (4) with respect to time from $t = 0$ to t taking into account equation (8) for $T_0 > T_m$, it is possible to obtain the law of energy conservation by a particle

$$E_T(t) - E_{T\infty} = Q_{ab} - Q_{en} - Q_{cond} - Q_{rad} - Q_m \tag{39}$$

where

$$E_{T\infty} = E_T(t=0)$$

$$Q_{en} = 4\pi \int_0^t \bar{j}(L_0 + C_0 T_0) r_0^2 \, dt.$$

When $T_0 < T_m$, the quantity Q_m is absent in equation (39). During numerical calculation of the system of equations control of the energy conservation law (39) was fulfilled which was satisfied with an error of $\leqslant 0.1\%$.

In Fig. 5 the quantities $\bar{c}_1$, $\bar{c}_2$ and $\bar{v}$ are presented vs time for several versions of calculation. The temperature increase and the evaporation of the particle at the initial stage $0 < t < t_m$ leads to the displacement of helium in the vicinity of the particle by aluminium vapours. A decrease of T_0 and of the evaporation rate when $t > t_{max}$ causes helium to return gradually back to the particle. The speed of convective motion $\bar{v}$ near the aluminium particle surface at $T_0 \approx T_m$ has characteristic values of $\sim 10^2$ m s^{-1} and is governed by the quantities T_0 and r_0 of the particle.

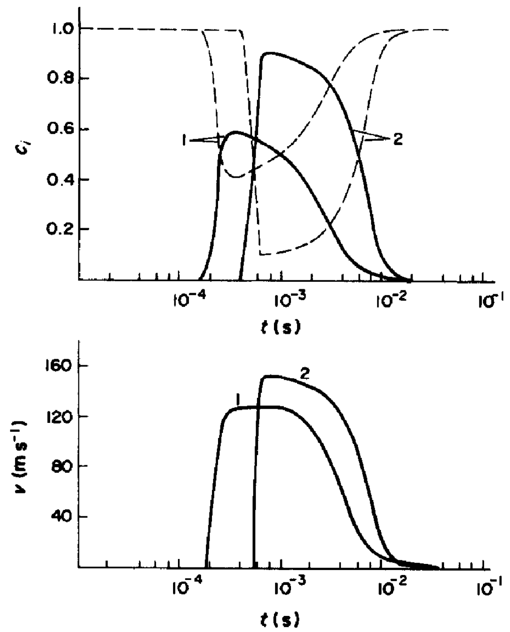

FIG. 5. The concentrations of vapour $\bar{c}_1$ (——), inert gas $\bar{c}_2$ (- - - - -) (a) and the velocity $\bar{v}$ (b) directly near the aluminium particle surface vs time t at $r_\infty = 10$ (1), 25 (2) μm and $I_0 = 0.5$ MW cm^{-2}.

4. HEATING AND COMBUSTION OF A HIGH-MELTING AEROSOL PARTICLE ON EXPOSURE TO OPTICAL RADIATION

Consider the heating and combustion of a high-melting metallic aerosol particle in an oxidant-containing gaseous medium on exposure to optical radiation. The specifics of the particle oxidation and combustion is that there is interaction between chemical and optical thermal bonds. The radiation intensity (energy Q_{ab}) determines the temperature of the particle T_0 and the rate of chemical reactions. The latter, in turn, determine the size and temperature of the particle and its absorptive properties. A metallic particle can burn in a low-temperature regime (when oxide film is formed on the particle surface in the process of ignition and combustion) and also in the high-temperature regime (when there is virtually no oxide film on the particle surface and the forming gaseous oxide is removed from the particle) [25]. In a general case, the gaseous medium surrounding the particle is a four-component mixture which includes the particle material vapours ($i = 1$), inert gas ($i = 2$), oxidant ($i = 3$) and gaseous oxide ($i = 4$), with $\sum_{i=1}^{4} c_i = 1$, and the particle may contain condensed metal (0) and oxide (ox). After the incorporation of the energy evolution due to radiation energy absorption and chemical reaction and energy losses by heat removal, radiative cooling and evaporation, the energy balance equation of a spherical particle with the instantaneous radius r_{ox}, which is equal to the radius of the outer surface of the oxide film, will have the form

$$(\rho_0 C_0 V_0 + \rho_{ox} C_{ox} V_{ox}) \frac{dT_0}{dt} = \left(\frac{I_0(t) K_{ab}}{4} - \bar{j} C_p \bar{T} - \bar{j}_{cond} - \bar{j}_{rad} - \bar{j}_{ev} - q_{ch} \bar{j}_3 \right) S_{ox} \tag{40}$$

whereas the balance equation of the metal and oxide masses in the particle, with oxidation and evaporation taken into account, have the form

$$\frac{\mathrm{d}(\rho_0 V_0)}{\mathrm{d}t} = -(\bar{j}_1 - \beta \bar{j}_3)S_{ox} \tag{41}$$

$$\frac{\mathrm{d}(\rho_{ox} V_{ox})}{\mathrm{d}t} = -(\bar{j}_4 + (1+\beta)\bar{j}_3)S_{ox} \tag{42}$$

where

$$V_{ox} = \tfrac{4}{3}\pi(r_{ox}^3 - r_0^3), \quad S_{ox} = 4\pi r_{ox}^2$$

β is the stoichiometric factor metal-oxidant [26], $h = r_{ox} - r_0$ is the thickness of the condensed oxide film on the particle. The initial and boundary conditions for equations (40)–(42) have the form

$$t = 0: \quad r_0 = r_{0\infty}, \quad r_{ox} = r_{ox\infty}, \quad T_0 = T_\infty,$$

$$c_i = 0, \quad i = 1,4; \quad c_i = c_{i\infty}, \quad i = 2,3 \tag{43}$$

$$h > 0, \quad r = r_{ox}: \quad \bar{j}_1 = 0, \quad \bar{j}_2 = 0,$$

$$\bar{j}_3 = -\frac{\rho_{ox}\bar{c}_3}{\dfrac{h}{D_k}\dfrac{r_{ox}}{r_0} + \dfrac{\rho_{ox}\exp(E_0/R_g T_0)}{\bar{\rho}k_0}} \tag{44}$$

$$\bar{j}_4 = \alpha_{ox}\left[\left(\frac{kT_0}{2\pi m_{ox}}\right)^{1/2}\rho_{ox\,sat} - \bar{c}_4\bar{\rho}\left(\frac{k\bar{T}}{2\pi m_{ox}}\right)^{1/2}\right],$$

$$\bar{j}_{ev} = \bar{j}_4 L_{ox};$$

$$h = 0, \quad r = r_0:$$

$$\bar{j}_1 = \alpha_0\left[\left(\frac{kT_0}{2\pi m_0}\right)^{1/2}\rho_{0sat} - \bar{c}_1\bar{\rho}\left(\frac{k\bar{T}}{2\pi m_0}\right)^{1/2}\right],$$

$$\bar{j}_2 = 0$$

$$j_3 = -k_0\bar{\rho}\bar{c}_3\exp(-E_0/R_g T_0),$$

$$\bar{j}_4 = -(1+\beta)\bar{j}_3, \quad \bar{j}_{ev} = \bar{j}_1 L_0 \tag{45}$$

when

$$r = \infty: \quad T = T_\infty, \quad c_i = 0, \quad i = 1,4;$$

$$c_i = c_{i\infty}, \quad i = 2,3. \tag{46}$$

In the presence of an oxide film on the particle surface, $h > 0$, there is no flow of metal vapours, the oxidant flow is proportional to the rate of heterogeneous reaction with regard for the diffusion of oxidant molecules to the metal through the condensed oxide film [26]; the flow of oxide vapours is determined by evaporation kinetics. In this case the system of equations (40)–(42) is calculated with equations (43), (44) and (46) taken into account. When there is no oxide film, $h = 0$, the flow of metal vapours is controlled by the evaporation kinetics, the oxidant flow is proportional to the heterogeneous reaction rate, the oxide flow is determined by the stoichiometry of the flow rates of metal and oxidant vapours. In this case equations (40) and (41) should be calculated taking into account equations (43), (45) and (46). There is no neutral gas flow in both cases. Also, the temperature jump near the burning particle surface is ignored, and the condition $T_0 = \bar{T}$ will be used in equations (44) and (45).

Consider the heating, oxidation and combustion of a boron particle in air at atmospheric pressure under the action of optical radiation at $T_\infty = 300$ K and assume that $c_{2\infty} = 0.8$, $c_{3\infty} = 0.2$ in equations (46).

The optical constants for boron are taken from ref. [27]; at $\lambda = 10.6$ μm and $T_\infty = 300$ K, $n_\lambda = 2.734$ and $\kappa_\lambda = 7.873 \times 10^{-2}$. Figure 1(b) presents the values of K_{ab} for boron particles calculated by the Mie theory, and also approximation (10) with $K_1 = 2.9 \times 10^3$ cm^{-1} and $K_2 = 3.45 \times 10^{-4}$ cm. An increase of n_λ for boron as compared to n_λ for water results in the situation that the use of approximation (10) leads to noticeable errors for $r_0 < 10$ μm as compared with the calculated K_{ab}. Consequently, relation (10) can be used when $n_\lambda - 1 < 1$ and $\kappa_\lambda \ll 1$. Unfortunately, the temperature dependencies of n_λ and κ_λ for water and boron are given only for narrow temperature ranges: $273 \leqslant T_0 \leqslant 323$ K for water [29] and $300 \leqslant T_0 \leqslant 873$ K for boron [27], thus making them inapplicable for describing the behaviour of particles in practically realizable and important ranges of T_0 variation (Figs. 2 and 6). Moreover, within these ranges of T_0 values, the magnitudes of n_λ, κ_λ and K_{ab} for water and boron are small ($\lesssim$2–10%), therefore for these quantities their values at $T_0 = T_\infty$ were used.

The values of the thermophysical parameters of boron and air, of transfer coefficients and constants for the heterogeneous chemical reaction of boron with air oxygen are borrowed from refs. [2, 6, 26, 28]. Figure 6 presents the time dependencies of T_0, r_0, r_{ox} for a boron particle with $r_{0\infty} = 14.9$ μm and $r_{ox\infty} = 15$ μm for two values of I_0. Investigation of the heating and combustion of a boron particle for the two values of I_0 given above allows the analysis of the high- and low-temperature regimes [30].

In the high-temperature regime with $I_0 = 10^4$ W cm^{-2}, when T_0 attains the boron melting temperature $T_m = 2348$ K, the particle is being melted within the time interval $\Delta t_m = 2 \times 10^{-3}$ s. Judging from equations (37) and from the boron densities in the solid $\rho_{0s} = 2.34 \times 10^3$ kg m^{-3}, and molten, $\rho_{0l} = 2.08 \times 10^3$ kg m^{-3}, states, there occurs an increase in the boron

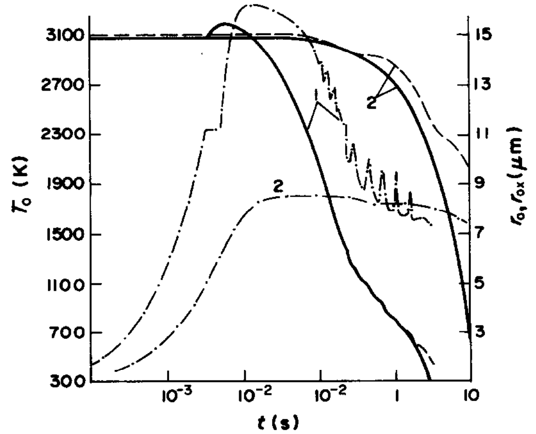

FIG. 6. The temperature T_0 (—·—·—), radii r_0 (——), r_{ox} (- - - -) of a boron particle vs time t at $r_{0\infty} = 14.9$ μm, $r_{ox\infty} = 15$ μm and $I_0 = 10^4$ (1), 2.85×10^3 (2) W cm^{-2}.

particle radius up to the value $r_{0l} = 1.04r_{0s}$. During the approach of T_0 to T_m and particle melting, an intensive evaporation of oxide from the particle surface begins, which is not compensated by oxide formation in the heterogeneous reaction on the metal surface. This leads to the disappearance of the oxide film, and the process of oxide evaporation is replaced by metal evaporation and by heterogeneous reaction between the metal and oxidant. With further heating, T_0 of the particle attains the maximum value $T_{max} = 3295$ K and then T_0 starts to decrease.

As r_0 decreases, $r_0 < 10$ μm, the particle behaviour in the optical radiation field becomes sensitive to the oscillating dependence of K_{ab} on r_0 for the boron particle (Fig. 1(b)). This leads to the appearance of oscillations of T_0 of the particle when it burns and its r_0 decreases. These oscillations correlate with the oscillations of K_{ab} on the axis of radii r_0. With a decrease of r_0, the amplitude of the oscillations of K_{ab} increases, and this causes a corresponding increase in the amplitude of oscillations of T_0 and, in turn, certain fluctuations in the function $r_0(t)$ (Fig. 6). The solidification of the boron particle during its cooling, which occurs at $r_0 \approx 6$ μm, leads to a corresponding decrease of r_0 (the discontinuity of the curve $r_0(t)$, Fig. 6). However, the solidification of the particle exerts a little effect on $T_0(t)$ and $r_0(t)$, since by this time the mass of the particle has decreased by more than an order of magnitude. A decrease of T_0 below ~ 1700 K causes the appearance on the particle of an oxide film which disappears during the subsequent temperature peak and then appears again, and its thickness increases.

In the low-temperature regime of boron particle combustion at $I_0 = 2.85 \times 10^3$ W cm^{-2}, the temperature T_0 attains the maximum value $T_{max} = 1805$ K in the process of heating and oxidation. In this case, evaporation of oxide begins and the oxide film disappears. However, as T_0 decreases, the oxide film appears again, with the oxide evaporation being compensated by its formation during reaction between metal and oxidant, and a certain stabilization of the oxide film thickness h on the particle takes place. Then, as r_{ox} and T_0 decrease, the oxide film thickness begins to increase due to a more rapid formation of oxide in chemical reaction, as compared with its evaporation, taking into account the fact that the oxide density $\rho_{ox} = 1.85 \times 10^3$ kg m^{-3} is smaller than the metal density. Thus, the oxide mass in the particle increases as a result of heterogeneous oxidation, and the mass of the metal decreases. The heat generated in this case in oxidation and the radiation energy absorbed by the particle slow down the rate of the decrease of T_0. Note, that in both regimes the melting of the initial oxide film at $T_m = 723$ K for boron oxide does not influence the function $T_0(t)$ and particle size, since the mass of the initial oxide film is negligibly small as compared with the mass of the metal. The solidification of the oxide film with a decrease of T_0 will influence the dynamics of the change in T_0 in the case when the mass of the oxide in the particle will be commensurable with (or higher than) the mass of the metal. In both regimes, the effect of the two-layered character of the particle, consisting of the metal core and of the surface oxide film, on its optical properties was taken into account. Correspondingly, the factors K_{ab} and K_{sc} in the process of combustion were calculated by the technique of ref. [31], with the optical properties of the metal and oxide [13, 27] for the instantaneous values of r_0, r_{ox} being taken into account and used in equations (40) and (8). It turned out in this case that the oxide film with the thickness $h \leqslant 0.1$–0.3 μm for $r_0 \gg h$ does not virtually influence the optical properties of the particle. At the same time, the increase of the oxide film thickness in the low-temperature regime up to the values $h \sim 1$–5 μm leads to a change in the optical properties of the particle, K_{ab} and K_{sc}, by about 20%, as compared with a metallic particle of the same size. It is of importance to take into account the change in the optical characteristics in the process of oxidation and combustion of particles in the optical radiation field.

The integration of equation (40) with respect to time from $t = 0$ to t, with equations (8) taken into account when $T_0 > T_m$, yields the energy conservation law for a burning particle

$$E_T(t) - E_{T\infty} = Q_{ab} + Q_{ch} - Q_{en} - Q_{cond} - Q_{rad} - Q_m. \tag{47}$$

In the process of numerical calculation the fulfilment of equation (47) was controlled with an error of $\leqslant 0.1\%$.

Figure 7 presents the time dependencies of energies Q and parameters M_i for two regimes of boron particle combustion. In the high-temperature regime an increase of the energy Q_{ev} when $t \gtrsim 10^{-3}$ s is associated with the oxide film evaporation. Then, Q_{ev} is constant for about 3×10^{-3} s due to the absence of metal evaporation in the process of heating up to T_m and particle melting. The evaporation of metal, occurring when $T_0 > T_m$, leads again to an increase of Q_{ev}. By the time $t \sim 3$ s, r_0 of the particle had decreased by about a factor of 10, the mass of the particle decreased respectively by about a factor of 10^3 and T_0 decreased below 1700 K. This causes the energies Q_{ev}, Q_{ch}, Q_{rad} to attain their steady-state values and the energy Q_{cond} to approach Q_{ab}, i.e. heat conduction removes virtually the entire absorbed energy from the particle.

In the low-temperature regime the increase of Q_{ev} up to the time $t \sim 10^{-1}$ s is associated with the oxide film evaporation. Then, during the time interval $\sim 2 \times 10^{-1}$ s, Q_{ev} is constant because of the absence of the oxide film and metal evaporation due to $T_0 < T_m$. The origination of an oxide film on the particle by the time $t \sim 5 \times 10^{-1}$ s and its evaporation lead again to the increase of Q_{ev}. By the time $t \sim 10$ s, the particle radius r_{ox} has decreased by about a factor of 1.5, and therefore all the energies still increase. Since T_0 is

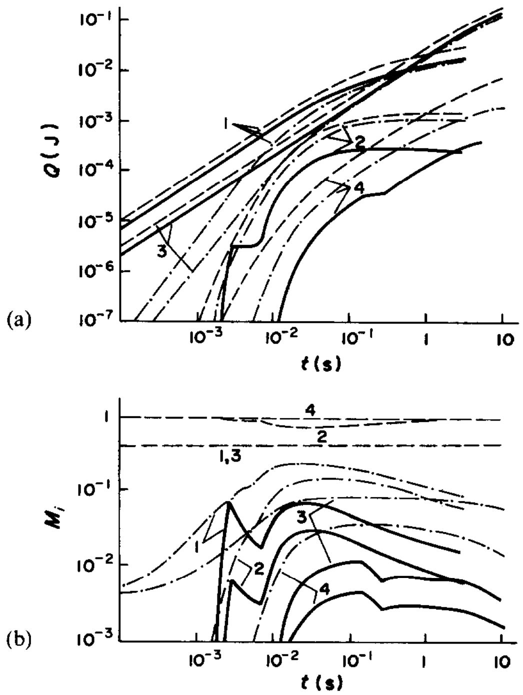

FIG. 7. The energies Q_{ab} (1, 3), Q_{ev} (2, 4)—solid lines, Q_{sc} (1, 3), Q_{rad} (2, 4)—dashed lines, Q_{cond} (1, 3), Q_{ch} (2, 4)—dashed-dotted lines (a) and the parameters M_1 (1, 3), M_2 (2, 4)—solid lines, M_3 (1, 3), M_4 (2, 4)—dashed lines, M_5 (1, 3), M_6 (2, 4)—dashed-dotted lines (b) vs time t for a boron particle with $r_{0\infty} = 14.9$ μm, $r_{ox\infty} = 15$ μm and $I_0 = 10^4$ (1, 2), 2.85×10^3 (3, 4) W cm^{-2}.

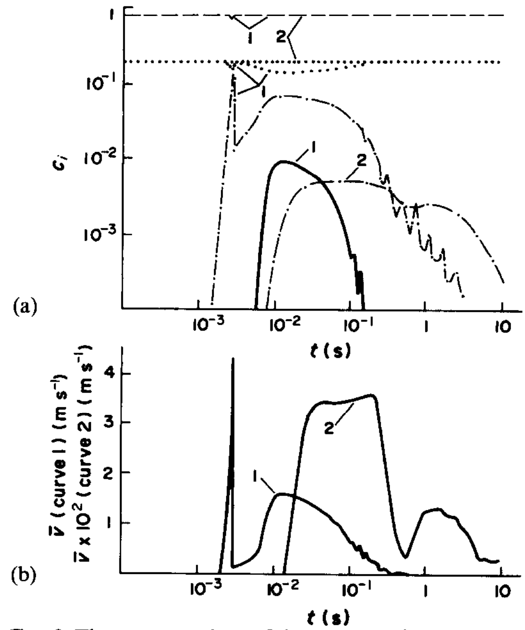

FIG. 8. The concentrations of the vapours of metal $\bar{c}_1$ (——), inert gas $\bar{c}_2$ (----), oxidant $\bar{c}_3$ (·····), oxide $\bar{c}_4$ (—·—) (a) and the velocity $\bar{v}$ (b) directly near the boron particle surface vs time t at $r_{0\infty} = 14.9$ μm, $r_{ox\infty} = 15$ μm and $I_0 = 10^4$ (1), 2.85×10^3 (2) W cm^{-2}.

comparatively small in this regime, $T_0 < 1800$ K, the energies Q_{rad} and Q_{ch} are much smaller than the energies Q_{ab} and Q_{sc}. In this case, the energy Q_{cond} removed by heat conduction from the particle, with the energies Q_{rad}, Q_{ch}, Q_{ev} taken into account, virtually completely compensates the energy generation Q_{ab} in the particle and this, taking into account the decrease of r_0, leads to a small decrease of T_0 with time.

The parameters M_1, M_4 and M_5 characterize the contribution of separate mechanisms of energy losses by the particle into its total energy balance. Characteristic discontinuities of the curves of M_1 and M_2 vs t are attributed to the presence of segments with $Q_{ev} \approx$ const. in the function $Q_{ev}(t)$. The parameter M_3 for a boron particle, just as for an aluminium particle, depends little on t and the estimation of M_3 from equation (38) gives in the present case $M_3 = 0.405$, in good agreement with the calculated data (Fig. 7). The parameter M_6 characterizes the contribution of the energy Q_{ch}, generated in chemical reaction, as compared with the energy Q_{ab} absorbed by the particle.

Figure 8 presents the quantities $\bar{c}_i$ and $\bar{v}$ vs time t for two regimes of particle combustion. In the high-temperature regime the concentration of metal vapours $\bar{c}_i$ near the particle surface, in the region of maximum T_0, attains the value $\bar{c}_1 \approx 10^{-2}$. The concentration of the oxidant $\bar{c}_3$ decreases in the region of maximum T_0 because of intensive absorption of oxidant in chemical reaction with metal. As T_0 decreases, when $t > 1 \times 10^{-1}$ s, $\bar{c}_3$ recovers its initial value. A sharp jump in the concentration of the gaseous oxide $\bar{c}_4$ at $t \sim 2 \times 10^{-3}$ s is associated with a very rapid (for the time $\sim 1 \times 10^{-3}$ s) evaporation of the initial oxide film on the particle. A short-time displacement of neutral gas and oxidant from the particle during this time interval takes place. A subsequent increase of $\bar{c}_4$ by the time $t \sim 10^{-2}$ s is associated with an intensive formation of a gaseous oxide in chemical reaction. Then, $\bar{c}_4$ and $\bar{c}_1$ decrease with characteristic oscillations due to the effect of $T_0(t)$ on the rates of evaporation and chemical reaction.

In the low-temperature regime $\bar{c}_1$ is virtually absent near the particle ($\bar{c}_1 < 10^{-4}$), $\bar{c}_3$ does not vary with time. The behaviour of $\bar{c}_4$ is similar to the function $T_0(t)$ in this regime. The concentration of the neutral gas $\bar{c}_2$ does not virtually vary in the process of particle combustion in both regimes.

In this case, the velocity of convective motion near the particle surface $\bar{v}$ has characteristic values of ~ 1 m s^{-1} and 4 cm s^{-1} for the high- and low-temperature regimes, respectively. Here, this is due to the fact that the characteristic temperatures, realized in these regimes, amount to $T_0 \lesssim 3200$ K and $T_0 \lesssim 1800$ K which are much smaller than the boiling temperature of boron and boron oxide. The behaviour of $\bar{v}$ is determined by the presence or absence of oxide film on the particle surface and also by the values of T_0 and r_0 in the process of combustion.

5. CONCLUSION

This paper has considered the heating, evaporation and combustion of a small-size solid aerosol particle in a gas on exposure to optical radiation. Actual temperature dependencies of the optical and thermophysical parameters of the particle material and gas and of transfer coefficients are taken into account when considering the quasi-steady-state diffusive–convective heat and mass transfer of a particle. The time dependencies of the radius and temperature of the particle and of the problem parameters in the process of evaporation and combustion are given. The results obtained may be of interest for investigating optical radiation propagation in dispersed media, for optical diagnostics of two-phase flows, etc.

REFERENCES

1. V. K. Pustovalov and G. S. Romanov, The theory of heating and evaporation of a spherical particle exposed to optical radiation, *Int. J. Heat Mass Transfer* **28,** 277–289 (1985).
2. I. K. Kikoin (Editor), *Tables of Physical Quantities* (*Handbook*). Atomizdat, Moscow (1976).
3. I. M. Alekseyev and P. N. Svirkunov, Evaporation from solid particles by laser radiation. In *Extended Abstracts of the 1st All-Union Meeting on Atmospheric Optics*, pt. 2, pp. 200–202. Izd. IOA SO AN SSSR, Tomsk (1976).
4. E. B. Belyaev, A. P. Godlevskiy and Yu. D. Kopytin, Laser spectrochemical analysis of aerosols, *Kvant. Elektronika* **5,** 2594–2601 (1978).
5. V. I. Igoshin and S. Yu. Pichugin, A chemical HF-laser induced by evaporation of fine-dispersed particles exposed to IR radiation, *Kvant. Elektronika* **10,** 1922–1924 (1983).
6. N. B. Vargaftik, *Handbook of Thermophysical Properties of Gases and Fluids*. Izd. Nauka, Moscow (1972).
7. V. I. Bukatyi, E. P. Zhdanov and A. M. Shaiduk, Concerning the combustion of aerosol particles in the electromagnetic radiation field, *Fiz. Gor. Vzryva* No. 3, 56–59 (1982).
8. Yu. I. Yalamov, E. P. Shchukin, L. G. Eidinov and Z. L. Shulimanov, Concerning the surface combustion of aerosol particles heated by inner heat sources, *Fiz. Gor. Vzryva* No. 4, 42–44 (1982).
9. V. K. Pustovalov and D. S. Bobuchenko, Problems of nonlinear heat conduction during optical radiation interaction with an absorbing particle. In *Proc. 7th All-Union Heat and Mass Transfer Conf., Heat Conduction*, pp. 49–53. Izd. ITMO AN BSSR, Minsk (1984).
10. V. K. Pustovalov and D. S. Bobuchenko, The dynamics of heating and cooling of a small particle in a gas medium, *Dokl. Acad. Nauk BSSR* **29,** 527–530 (1985).
11. V. K. Pustovalov and D. S. Bobuchenko, Investigation of nonlinear heat transfer between a spheroidal particle heated by optical radiation and the surrounding medium, *Dokl. Acad. Nauk BSSR* **30,** 513–516 (1986).
12. A. P. Prishivalko, *Optical and Thermal Fields Inside Light-scattering Particles*. Izd. Nauka i Tekhnika, Minsk (1983).
13. V. N. Zolotaryov, V. N. Morozov and E. V. Smirova, *Optical Constants of Natural and Technical Media*. Izd. Khimiya, Leningrad (1984).
14. G. N. Plass, Temperature dependence of Mie, scattering and absorption cross-sections for aluminum oxide, *Appl. Opt.* **4,** 1616–1619 (1965).
15. Yu. K. Lingart, V. A. Petrov and A. A. Tikhonova, Optical properties of leucosaphire at high temperature, *Teplofiz. Vysok. Temp.* **20,** 872–880, 1085–1092 (1982).
16. V. Ya. Klabukov, L. T. Grebenschikov, V. A. Kudryavtsev and M. A. Ivashevskiy, Experimental investigation of the optical properties of leucosaphire at high temperatures, *J. Engng Phys.* **47,** 332 (1984).
17. J. V. Dave, Scattering of electromagnetic radiation by a large, absorbing sphere, *IBM J. Res. Dev.* No. 5, 302–313 (1969).
18. W. L. Lentz, Generating Bessel function in Mie scattering calculations using continued fractions, *Appl. Opt.* **15,** 668–671 (1976).
19. D. S. Bobuchenko and V. K. Pustovalov, Temperature dependence of the 0.63 and 1.06 μm radiation absorption and scattering efficiency factors of spherical aluminum oxide particles, *Zh. Prikl. Spektr.* **44,** 335 (1986).
20. H. C. van de Hulst, *Light Scattering by Small Particles*. Wiley, New York (1957).
21. V. K. Pustovalov, Diffusive–convective evaporation of a droplet by intensive optical radiation with account for the temperature dependence of transfer coefficients, *J. Engng Phys.* **30,** 718–724 (1986).
22. E. V. Ivanov and V. Ya. Korovin, Water droplet evaporation in a continuous CO_2 laser radiation field, *J. Engng Phys.* **34,** 807–812 (1978).
23. I. L. Zelmanovich and K. S. Shifrin, *Tables of Light Scattering*. Vol. 3. *Coefficients of Attenuation, Scattering and of Light Pressure*. Gidrometeoizdat, Leningrad (1968).
24. V. I. Konov and V. N. Tokarev, Temperature dependence of the absorptivity of aluminum targets at the 10.6 μm wavelength, *Kvant. Elektronika* **10,** 327–331 (1983).
25. V. N. Gremyachkin, A. G. Istratov and O. N. Leipunskii, Concerning the combustion of metallic particles. In *Physical Processes in Combustion and Evaporation*, pp. 4–67. Atomizdat, Moscow (1980).
26. E. A. Zolotar and E. S. Ozerov, About the calculation of the boron particle ignition limit, *Fiz. Gor. Vzryva* **9,** 515–521 (1973).
27. J. Jaumann and H. Werheit, Optical absorption and photoelectrical effects in β-rhombohedral boron, *Boron* **3,** 227–245 (1970).
28. M. E. Drits (Editor), *Properties of Elements* (*Handbook*). Izd. Metallurgiya, Moscow (1985).
29. L. W. Pinkleu, P. P. Sethua and D. Williams, Optical constants of water in the infrared. Influence of temperature, *J. Opt. Soc. Am.* **67,** 494–499 (1977).
30. V. K. Pustovalov and D. S. Bobuchenko, Combustion of a high-melting aerosol particle in the optical radiation field. In *Physical and Chemical Processes in Non-equilibrium Systems*, pp. 99–105. Izd. ITMO AN BSSR, Minsk (1986).
31. A. P. Prishivalko and L. G. Astafieva, *Absorption, Scattering and Attenuation of Light by Water-clad Atmospheric Aerosol Particles*, Preprint of the Institute of Physics of the BSSR Academy of Sciences, Minsk (1975).

CHAUFFAGE, EVAPORATION ET COMBUSTION D'UN AEROSOL SOLIDE DANS UN GAZ SOUMIS A UN RAYONNEMENT OPTIQUE

Résumé—On étudie théoriquement le chauffage, l'évaporation et la combustion d'un aérosol de petites particules solides dans un gaz exposé à un rayonnement optique intense. On pose le problème et la solution est obtenue pour le transfert permanent de chaleur et de masse entre la particule et le gaz environnant en tenant compte de la variation avec la température des paramètres thermophysiques et optiques et des coefficients de transfert. A partir de la solution numérique du système d'équations, on considère l'évaporation d'une particule de métal dans un gaz inerte et la combustion d'une particule fusible dans l'air avec exposition à un rayonnement optique. On obtient la variation dans le temps du rayon et de la température de la particule. On compare quelques résultats obtenus à des données expérimentales.

AUFHEIZUNG, VERDAMPFUNG UND VERBRENNUNG EINES AEROSOL-PARTIKELS BEI OPTISCHER BESTRAHLUNG

Zusammenfassung—Es wurden theoretische Untersuchungen bezüglich des Aufheiz-, Verdampfungs- und Verbrennungsvorganges eines kleinen Aerosol-Partikels bei intensiver optischer Bestrahlung durchgeführt. Dazu wird ein Lösungsansatz vorgestellt und die Lösung für quasistationären Wärme- und Stoffübergang, infolge von Diffusion und Konvektion zwischen Partikel und umgebendem Gas ermittelt. Die Temperaturabhängigkeit der thermophysikalischen und optischen Parameter, sowie der Übergangskoeffizienten wird berücksichtigt. Basierend auf der numerischen Lösung des Gleichungssystems wird die Verdampfung eines Metallpartikels in einem Inertgas, sowie die Verbrennung eines schwer schmelzenden Partikels in Luft bei optischer Bestrahlung bestimmt. Es wird die zeitliche Veränderung von Radius und Temperatur des Partikels, sowie der Prozeßparameter untersucht. Vergleiche mit experimentellen Daten werden angegeben.

НАГРЕВ, ИСПАРЕНИЕ И ГОРЕНИЕ ТВЕРДОЙ АЭРОЗОЛЬНОЙ ЧАСТИЦЫ В ГАЗЕ ПОД ДЕЙСТВИЕМ ОПТИЧЕСКОГО ИЗЛУЧЕНИЯ

Аннотация—Теоретически исследованы нагрев, испарение и горение твердой аэрозольной частицы малого размера, находящейся в газе, под действием интенсивного оптического излучения. Приведена постановка задачи и получено решение для квазистационарного диффузионно–конвективного тепломассообмена частицы с окружающим газом с учетом температурных зависимостей теплофизических и оптических параметров, коэффициентов переноса. На основе численного решения сформулированной системы уравнений рассмотрены испарение металлической частицы в инертном газе и горение тугоплавкой частицы в воздухе под действием оптического излучения. Получены зависимости радиуса и температуры частицы, параметров процесса от времени. Проведено сравнение некоторых результатов расчетов с экспериментальными данными.